Relationship Between the Crystalline Structure and Mechanical Behavior in Isotropic and Oriented Polyamide 12

Nadya Dencheva,[1] Zlatan Denchev,[1] M. Jovita Oliveira,[1] Teresa G. Nunes,[2] Sérgio S. Funari[3]

[1]*Institute for Polymers and Composites, Department of Polymer Engineering, University of Minho, Guimarães, Portugal 4800-058*
[2]*Department of Materials Engineering, Instituto Superior Técnico, Av. Rovisco Pais 1, Lisbon, Portugal 1049-001*
[3]*Hamburger Synchrotronstrahlungslabor, Deutsches Elektronen-Synchrotron, Notkestraße 85, Hamburg, Germany 22603*

Received 10 September 2007; accepted 3 November 2007
DOI 10.1002/app.27938
Published online 28 March 2008 in Wiley InterScience (www.interscience.wiley.com).

ABSTRACT: This study reports on the relationship between the crystalline structure and mechanical behavior of differently processed and annealed polyamide 12 (PA12) samples. Two sets of samples were obtained: isotropic PA12 films prepared by hot pressing and oriented cables prepared by consecutive extrusion and cold drawing. These samples were isothermally annealed in the range of 80–160°C and then subjected to tensile tests at room temperature. A combination of solid-state ^{13}C-NMR and synchrotron wide- and small-angle X-ray scattering was used to obtain reliable structural data from these samples before and after the tensile tests. These structural data were related to the mechanical properties of the respective PA12 samples. Deformation models explaining all the experimental results were suggested for the different PA12 samples. © 2008 Wiley Periodicals, Inc. J Appl Polym Sci 109: 288–302, 2008

Key words: mechanical properties; polyamides; polymorphism; SAXS; WAXS

INTRODUCTION

The properties of polyamide 12 (PA12) represent a valuable combination of typical nylon and polyolefin properties, such as low moisture absorption and density accompanied by chemical resistance similar to that of polyamide 6 (PA6) with lower sensitivity to stress cracking.[1,2] PA12 shows excellent impact strength and high Young's modulus (E) values. All this makes PA12 an important engineering plastic with a multiplicity of applications in technical engineering, especially in the automotive and electrical industries.[3] Therefore, studying the relationship between the PA12 structure and its mechanical properties has always been of both practical and academic interest.

It is generally accepted that polyamides possess layerlike structures formed by hydrogen-bonded sheets. The two basic crystalline modifications, designated the α and γ forms, were established for the first time in PA6.[4–7] It has been demonstrated that, similarly to PA6, PA12 may also crystallize in α- and γ-crystalline modifications, the latter being the more stable polymorph.[8] Depending on the crystallization conditions, four PA12 polymorphs have been reported, and they are designated α, α′, γ, and γ′. The main crystalline form obtained by the melt crystallization of PA12 at atmospheric pressure is the γ form, whereas the polymorph obtained by cryogenic quenching from the melt and subsequent crystallization at 60°C is denoted the γ′ modification.[9] The α polymorphs of PA12 are obtained under special conditions, such as crystallization from the melt at a pressure above 500 MPa,[10] precipitation from a phenol–ethanol solution,[11] or drawing close to the melting point.[12]

With respect to the transitions between the four PA12 polymorphs, it has been reported that thermal treatment under pressure gives rise to a γ′-to-α transition, whereas under the same conditions, no change in the γ-crystalline form has been established.[10,13] The γ′ structure can be transformed also into the α form through annealing above 110°C at

Correspondence to: Z. Denchev (denchev@dep.uminho.pt).
Contract grant sponsor: Improving Human Potential (IHP), European Commission; contract grant number: HPRI-CT-2001-00140.
Contract grant sponsor: Hamburger Synchrotronstrahlungslabor; contract grant number: II-04-047 EC.
Contract grant sponsor: Fundação para a Ciência e Tecnologia (Portugal) [FCT]; contract grant number: POCI/CTM/57358/2004.
Contract grant sponsor: Fundação para a Ciência e Tecnologia (Portugal); contract grant number: SFRH/BD/13435/2003 (to support the Ph.D. research of N.D.).

atmospheric pressure.[13] The effect of drawing on the crystalline structure of PA12 was studied for the first time by means of wide-angle X-ray scattering (WAXS) by Northolt et al.[14] The difference in the WAXS patterns before and after drawing was attributed to two different crystalline forms. Hiramatsu et al.[13] reported later that drawing above 50 and 70°C could result in γ-γ′ and α–γ′ transitions, respectively. Ishikawa et al.[12] observed a partial γ-to-α-form transition while drawing PA12 samples at temperatures near the melting point.

Our own studies on the structure of PA12 showed some differences in the polymorphic transitions occurring in the isotropic γ form and in the oriented γ′ form. Upon heating above 140°C, the isotropic γ polymorph partially changed into α-PA12, which only existed at a high temperature and rapidly changed back into the γ form when cooled. No such γ-to-α transformation was observed with the oriented γ′-PA12 phase even after annealing at temperatures close to melting. A γ′-to-γ transition was observed here only after isotropization by melting.[15]

This article is a part of a broader study on the structure–property relationship in *in situ* composite materials based on polymer blends containing PA12. It reports on the mutual relationship between the structure in the crystalline and amorphous domains and the mechanical behavior in well-characterized, differently annealed, oriented or isotropic PA12 samples containing various amounts of α and γ polymorphs. To the best of our knowledge, no such studies have been published so far with PA12. The influence of the starting structure on the mechanical properties of PA12 samples is studied. Then, the influence of strain after sample failure on the changes in the crystalline and amorphous phases is elucidated. Synchrotron WAXS and small-angle X-ray scattering (SAXS) have been used, complemented by solid-state ^{13}C-NMR spectroscopy, which allows the verification of the types and contents of the respective polymorphs.

EXPERIMENTAL

Materials used and sample preparation

High-viscosity-grade PA12, obtained by ring-opening polymerization and commercially available under the trade name Grilamid L25 (EMS Grivory, Domat/Ems Switzerland) with a density of 1.01 g/cm^3, a weight-average molecular weight of 60.000, a number-average molecular weight of 31.000, and a melting point of 178°C (differential scanning calorimetry), was used as a starting material.

Two types of PA12 samples were prepared and studied. The first set of samples, designated as isotropic films, was obtained by compression molding of as-supplied granules preliminarily dried for 5 h at 90°C. The starting material was pressed at 250°C, and a pressure of 6 tons was applied for 5 min; this was followed by isothermal crystallization for 1 h at three different temperatures: 120, 140, or 160°C. An additional sample was prepared with 3 h of isothermal crystallization at 120°C. After the annealing was completed, 200–250-μm-thick films were prepared by cooling to room temperature at a rate of about 20°C/min. Five standard specimens for tensile stress measurements, 25 mm long and 4 mm wide, were cut out from each film.

The second set of samples, designated as oriented cables (OCs), was prepared in an extruder line including a Lestritz LSM 30.34 Nuremberg, Germany intermeshing, corotating twin-screw extruder, two water baths, two haul-off units, and a winder positioned downstream. The extrusion was performed at a set temperature of 230°C. The extrudate was cooled in the first water bath down to 12°C while being drawn at a draw ratio of approximately 3.0. The final drawing was performed in the second haul-off unit after heating of the stretched cable up to 90–96°C in the second water bath. More details about the extruder line can be found elsewhere.[16] The PA12 OCs were annealed with free ends at 80, 100, 120, and 160°C in an oven. After 1 h of annealing at the respective temperature, the sample was cooled at about 10°C/min until it returned to room temperature. Major sample contraction was observed at each annealing temperature with all PA12 OCs.

Solid-state NMR

Solid-state NMR measurements were performed in a Bruker (Billerica, MA) MSL300P spectrometer operating at 75.47 MHz for the observation of ^{13}C resonances with magic-angle spinning (MAS), high-power ^{1}H dipolar decoupling (DD), and ^{1}H–^{13}C cross-polarization (CP) combined techniques. The ^{1}H–^{13}C CP contact time was 1 ms, giving a good discrimination of the protonated signals. The maximum inter-radio-frequency pulse sequence delay was 3.0 s at a spinning rate of 3.4 kHz. The B_1 radio-frequency field intensity was 55 kHz, and the number of scans varied between 1000 and 2000. Glycine signals were employed as external references for the determination of the chemical shifts with an accuracy of 0.2 ppm. The temperature of the probe head was set to 20 ± 1°C. The experimental spectra were fitted by individual Gaussian peaks with commercial peak-fitting software.

WAXS and SAXS measurements

Synchrotron radiation with a wavelength of 0.15 nm, generated at the soft condensed matter beam line (A2) of Hamburger Synchrotronstrahlungslabor

(Hamburg, Germany), was employed. The first setup permitted two-dimensional (2D) SAXS and one-dimensional (1D) WAXS measurements. The sample-to-detector distance for SAXS was set to 2850 mm, the diffraction patterns being registered by means of a Charge Coupled Device detector (MARCCD) manufactured by Rayonix (Evanston, IL) 2D detector with exposure times between 30 and 90 s. The 1D WAXS profiles were registered by a linear scintillation detector positioned at 240 mm with respect to the sample holder. In the second setup for 2D WAXS, the linear detector was removed, and the MARCCD detector was positioned at 90 mm from the sample. More details on the setups employed may be found elsewhere.[15]

SAXS and WAXS data handling

Data handling procedures were performed as previously described.[15–18] All SAXS and WAXS patterns were corrected for background scattering, constant sample thickness, and beam intensity. The scattering angle axis for WAXS was calibrated with the angular position of the reflections of a standard crystalline poly(ethylene terephthalate) sample. Calibration of the SAXS scattering angle axis was made with a rat-tail standard sample.

All WAXS curves were fitted with Gaussian peaks. In the case of isotropic PA12, the total degree of crystallinity [or crystallinity index (CI_{total})] was calculated as a relation of the areas of all crystalline peaks and the total area underneath the WAXS curve:

$$CI = \frac{\sum A_c}{\sum (A_c + A_a)} \quad (1)$$

where A_c is the integrated area underneath the respective crystalline peaks and A_a is the integrated area of the amorphous halo.

In PA12 OCs, the intensity of the meridional pointlike reflections cannot be determined from the 1D WAXS curves. In this case, $\sum A_c$ in eq. (1) measures the scattering intensity along the equator only; that is, eq. (1) would represent the equatorial crystallinity index (ECI).

The 1D WAXS patterns were used also to determine the interplanar spacings d_{h00} and d_{00l} with Bragg's law:

$$2d_{hkl} \sin \theta_{hkl} = \lambda \quad (2)$$

where λ = 1.5 Å is the X-ray wavelength and θ is half of the 2θ position of the center of the respective crystalline peak.

Tensile tests

Uniaxial tensile tests were performed in an Instron model 4505 machine (Norwood, MA). The tests were carried out at 23 ± 2°C with a load cell of 1 kN at a constant crosshead speed of 50 mm/min. The nominal stress was determined as a ratio of the tensile force to the initial cross section of the sample. The nominal strain was determined as a ratio of the sample gauge length at any time during drawing to that before drawing.

RESULTS

Mechanical data

Figure 1(a,b) shows the stress–strain curves of differently annealed isotropic PA12 films and OCs, respectively. All data extracted from these curves are presented in Table I.

As shown in Figure 1(a), all isotropic PA12 samples displayed clear yield points at low strains (between 7 and 9%) and cold flow regions, a behav-

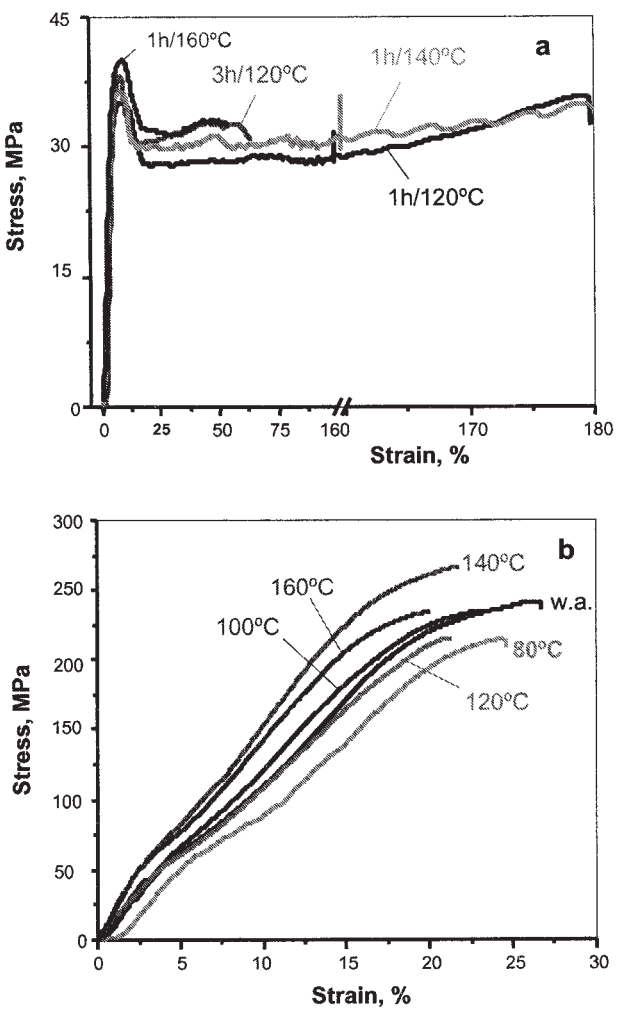

Figure 1 Stress–strain curves of various PA12 samples: (a) isotropic films annealed for 1 h at 120, 140, or 160°C and for 3 h at 120°C and (b) oriented PA12 cables without annealing (w.a.) or annealed at 80, 100, 120, and 140°C for 1 h. The curves were selected to best fit the averaged data in Table I.

TABLE I
Tensile Properties of Isotropic and Oriented PA12 Samples After Various Annealing

Sample and annealing conditions	E (GPa)	σ_y (MPa)[a]	Yield strain (%)	Maximum stress (MPa)	Strain at maximum stress (%)	σ_{br} (MPa)	ε_{br} (%)
PA12 films							
120°C/1 h	0.83 ± 0.07	32 ± 3	8.1 ± 0.5	33 ± 10	188 ± 16	33 ± 8	189 ± 20
120°C/3 h	1.01 ± 0.10	34 ± 5	6.9 ± 0.1	35 ± 6	7 ± 2	27 ± 6	63 ± 5
140°C/1 h	0.89 ± 0.07	32 ± 1	8.3 ± 0.6	34 ± 6	200 ± 11	35 ± 9	203 ± 13
160°C/1 h	1.03 ± 0.06	36 ± 1	8.7 ± 0.5	36 ± 3	9 ± 1	28 ± 7	54 ± 6
PA12 OCs							
Without annealing	1.63 ± 0.08	56 ± 1	4.2 ± 0.4	241 ± 10	26 ± 3	235 ± 7	27 ± 3
		220 ± 2	18.7 ± 1.0				
80°C/1 h	1.23 ± 0.16	53 ± 1	4.9 ± 0.3	215 ± 6	24 ± 2	209 ± 7	25 ± 2
		207 ± 2	21.3 ± 1.4				
100°C/1 h	1.67 ± 0.07	45 ± 1	2.9 ± 0.2	234 ± 3	23 ± 2	233 ± 10	23 ± 3
		227 ± 2	18.5 ± 1.1				
120°C/1 h	1.46 ± 0.10	50 ± 2	3.6 ± 0.2	216 ± 8	21 ± 2	214 ± 9	21 ± 2
		213 ± 2	19.6 ± 1.5				
140°C/1 h	2.19 ± 0.12	59 ± 2	2.9 ± 0.1	266 ± 10	21 ± 3	265 ± 10	22 ± 2
		254 ± 3	16.5 ± 0.9				
160°C/1 h	2.24 ± 0.15	58 ± 1	2.8 ± 0.2	234 ± 8	20 ± 1	233 ± 11	20 ± 1
		230 ± 3	16.5 ± 0.8				

[a] OCs displayed two yield points.

ior typical of necking. The samples annealed at 120°C for 1 h and at 140°C failed at a strain at break (ε_{br}) of approximately 200%, whereas the other two films broke at ε_{br} values of 50–60%. Table I shows that the isotropic PA12 samples displayed a slight augmentation of E from 830 to 890 to 1030 MPa. This effect was achieved by increases in either the annealing temperature from 120 to 160°C or in the duration of the treatment from 1 to 3 h at 120°C. The yield stress (σ_y) values of all isotropic samples were between 32 and 36 MPa, the highest value corresponding to the highest annealing temperature of 160°C. It can be concluded that annealing results in a harder PA12 film.

Figure 1(b) shows that all the oriented PA12 cables were characterized by two yield points. As seen from the data in Table I, the first yields appeared at low strains (3–5%) with σ_y values between 45 and 59 MPa. At strains of 16–21%, one can recognize in all OCs a second yield point with σ_y values of 207–254 MPa. A statistically significant increase in the E values here was reached only at annealing temperatures of 140 and 160°C; at lower temperatures, the mechanical behavior of the annealed OCs was similar to that of the OC without annealing.

Solid-state ^{13}C-NMR data

In our previous study,[15] the solid-state NMR spectra of PA12 granules and PA12 cables obtained through the melting of the same granules in a melt flow index apparatus followed by stretching at approximately 100°C did not reveal any resonance lines above 40 ppm and also no peaks around 38.9–39.0 ppm. On this basis, the presence of the α polymorph in both samples was ruled out. For the mechanical experiments in this work, isotropic films were prepared by hot pressing, and OCs were prepared with the extruder line with two stretching devices. The MAS/CP–DD ^{13}C-NMR spectra of a PA12 isotropic film annealed for 1 h at 160°C and of the new OC with the same thermal prehistory obtained before and after the tensile testing of the samples were visibly different from those of the previous study. Having in mind also the prolonged annealing of the samples at elevated temperatures, we decided to analyze the new NMR data by peak fitting, supposing the presence of both α- and γ-PA12 polymorphs. This hypothesis was based on the previous works reporting on a γ-to-α-form transition upon cold drawing[12] or pressing.[13] The crystallinity data obtained by the fitting of the NMR curves were then correlated with the X-ray scattering results.

Fitting of the NMR spectra is made on the basis of the four types of aliphatic carbons found in the repeat unit of both α-PA12 and γ-PA12 (Table II).

In each polymorph, the eight CH_2 methylenes (type c carbons) coexist in all-trans and gauche (skewed) conformations, the resonances of these structures being in the 30.3–34.3 ppm range. The methylene type b carbon, being the most electron-shielded, appears in stronger fields of approximately 27 ppm. As expected, the carbon located next to the C=O and that next to the NH group (types a and d, respectively) produce resonance lines in weaker fields (up to 43 ppm).

Figures 2 and 3 present the fittings of the extended methylene carbon regions of an isotropic PA12 sample annealed for 1 h at 160°C and an OC with the

TABLE II
Solid-State ^{13}C-NMR Analysis of PA12 Isotropic and Oriented Samples Annealed for 1 h at 160°C Before and After Tensile Testing (Aliphatic C Region)

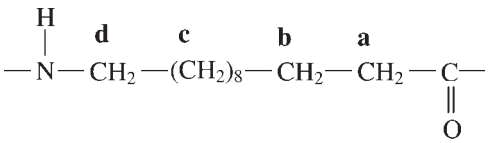

	Chemical shift (ppm)				
NMR resonance	PA12 from ref. 19	PA12 film	PA12 film after tensile testing	PA12 OC	PA12 OC after tensile testing
b γ form (γ′ form)	~ 28 (~ 27)	26.5[a]	25.1	26.4[a]	25.3
b (α form)	27.3		26.7		26.7
c gauche γ form	30.3	29.9	29.7	29.7	30.0
c gauche γ′-form	30.8				
c gauche (α form)	30.9	31.6	31.4	31.6	31.4
c trans (γ form)	33.6	32.8	32.5	32.8	32.8
c trans (γ′ form)	33.1				
c trans (α form)	34.2	34.4	34.2	34.6	34.5
a (γ form)	37.3	36.3	36.5	36.5	36.6
a (γ′ form)	37.0				
a (α form)	38.9	37.4	—[b]	—[b]	—[b]
d (γ form)	39.8	39.8	40.2	39.5	39.9
d (γ′ form)	40.3				
d (α form)	43.0	42.2	42.7	42.1	42.8
α/γ content	—	0.19	0.27	0.24	0.52

[a] The resonances of the corresponding nucleus of the α and γ forms cannot be separated.
[b] Fitting does not suggest a resonance peak in this region in oriented samples.

same thermal history before and after tensile testing. The respective chemical shifts obtained after the peak fitting for all types of carbons are presented in Table II. They are very close to those found previously.[19]

Fitting the NMR spectra allowed the calculation of the α/γ polymorph ratio, which was done in the following way. The areas of all-cis and all-trans methylene carbon γ-PA12 peaks were summed and divided by 8, and in such a way, the integral intensity corresponding to one γ-carbon was obtained. This value was then used to divide the integral intensity of the d-type carbon of α-PA12. One has to mention that it is possible to calculate the α/γ ratio relating the intensity of any NMR signal of a carbon belonging to α-PA12 to that of any carbon of the γ phase. In all cases, very similar values were obtained. We preferred to use the signal of the α-PA12 d-carbon for two reasons. This signal appears above 40 ppm, where there are no γ-form signals whatsoever, so its presence undoubtedly proves the α form. Below 40 ppm, superposition is possible between α- and γ-form signals. The second reason was the better agreement with the WAXS data.

1D WAXS measurements

As seen from the comparison between the literature and our chemical shift data presented in Table II, in isotropic PA12 films and PA12 OCs, a clear distinction is possible between the α- and γ-PA12 phases. However, no distinction is possible between the γ- and γ′-PA12. That is why in this work, when referring to oriented PA12 samples, we will have in mind the γ′-oriented PA12 phase; the isotropic PA12 films will be considered then as containing the γ-type isotropic phase only.

Figure 4 shows the fitted 1D WAXS patterns of the same isotropic and oriented PA12 samples studied by solid-state NMR. All fits were made with five Gaussians, two for the monoclinic α polymorph, two for the pseudohexagonal γ-type isotropic polymorph, and one broad peak for the amorphous halo. Comparing the shapes of the patterns allows the conclusion that the isotropic PA12 and oriented PA12 have different crystalline structures. The centers of the amorphous halo in the isotropic sample [Fig. 4(a)] do not coincide with the main crystalline peaks as in PA12 with orientation [Fig. 4(b–d)].

From the shapes of the 1D WAXS patterns of the oriented samples, it is not straightforward whether or not they should be fitted with crystalline peaks for the α phase. This becomes evident only on the basis of the NMR results shown in Table II. It is worth noting that the α/γ ratios obtained from the WAXS patterns of the isotropic and oriented PA12 samples annealed at 160°C before and after tensile testing almost coincide with those obtained for the

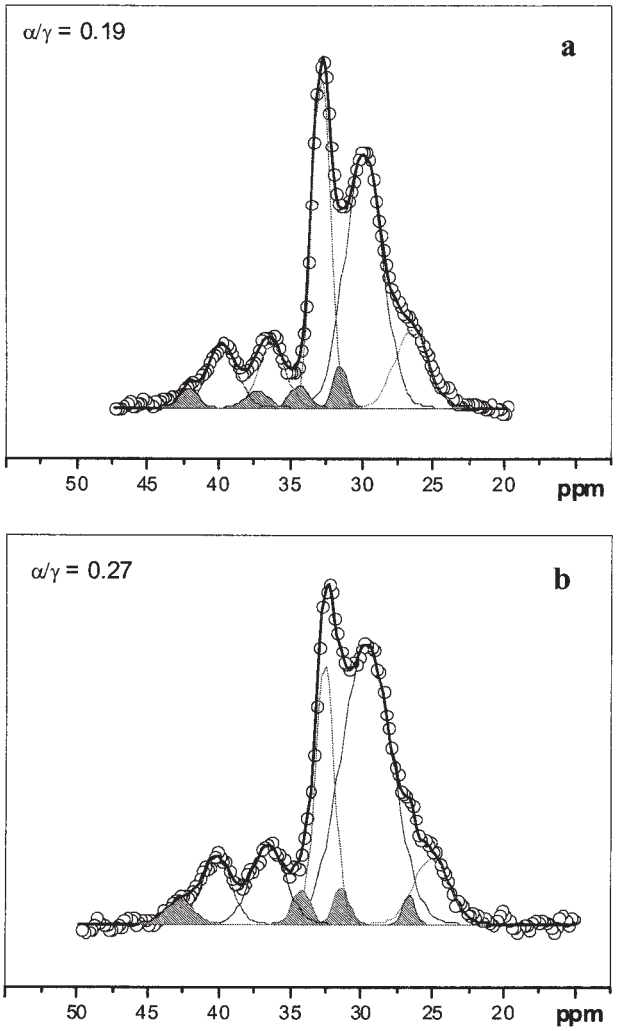

Figure 2 Aliphatic atom region of the MAS/CP–DD ^{13}C spectra at 20°C of an isotropic PA12 film annealed for 1 h at 160°C: (a) before and (b) after tensile testing. The resolved resonance lines of α-PA12 are shaded. The chemical shifts of all resonance lines are given in Table II.

same samples by the fitting of their NMR patterns. Therefore, the procedure of fitting these particular WAXS curves was extended to all 1D WAXS patterns. The structural data obtained in such a way are presented in Table III.

As shown in Table III, the annealing of isotropic PA12 samples resulted in a small increase of CI, which is better expressed for the γ crystals. Stretching during the tensile test resulted, as a rule, in strain-induced crystallization of amorphous material predominantly in the α form. With the PA12 OCs, when the annealing temperature was increased in the 80–140°C range, a significant increase in ECI of approximately 11% was produced. The small drop in ECI at 160°C, which is 15° below the melting point of PA12, should be attributed to some melting/recrystallization processes. The tensile test with the differently annealed OCs resulted in a general γ-to-α-form transition, with almost the same ECI values maintained as before the tensile test.

2D WAXS measurements

The CI values in Table III and most of the *d*-spacing data in Table IV were obtained on the basis of the 1D WAXS patterns. The latter, however, account only for the equatorial WAXS reflections. It is known from previous studies that oriented γ-PA12 also displays meridional pointlike reflections. Therefore, 2D WAXS patterns were obtained from which the $d_{\gamma 020}$ values were determined for some PA12 samples, before and after tensile testing. The most representative 2D WAXS patterns are shown in Figure 5.

The first pattern in Figure 5 is isotropic. The equatorial cut of its external ring produces the pattern in Figure 4(a). The internal ring is related to $d_{\gamma 020}$ and is also quite isotropic. The pattern in Figure 5(b)

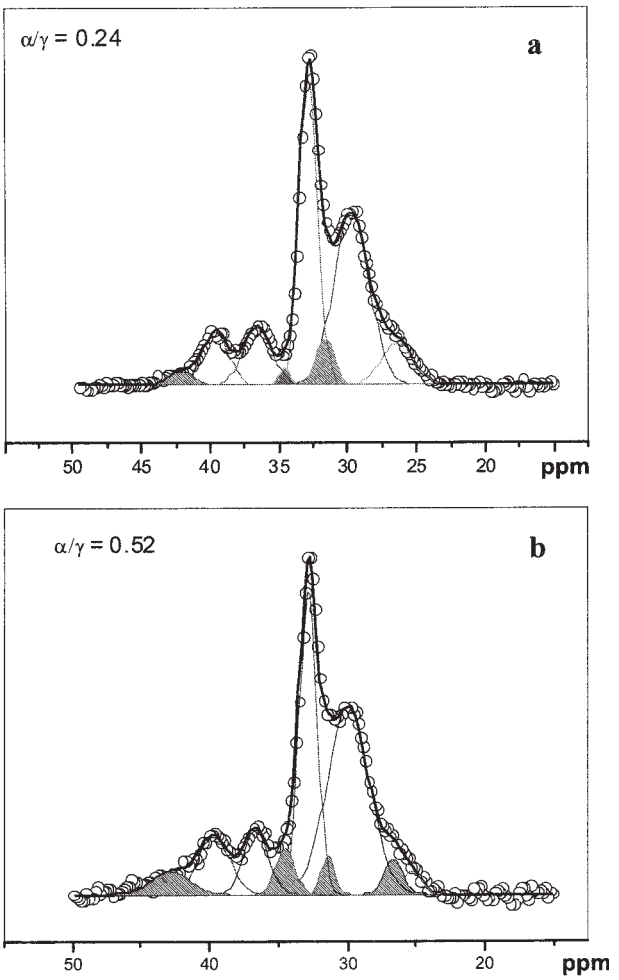

Figure 3 Aliphatic atom region of the MAS/CP–DD ^{13}C spectra at 20°C of PA12 OC obtained by extrusion/cold drawing and annealed for 1 h at 160°C: (a) before and (b) after tensile testing. The resolved resonance lines of α-PA12 are shaded. The chemical shifts of all lines are given in Table II.

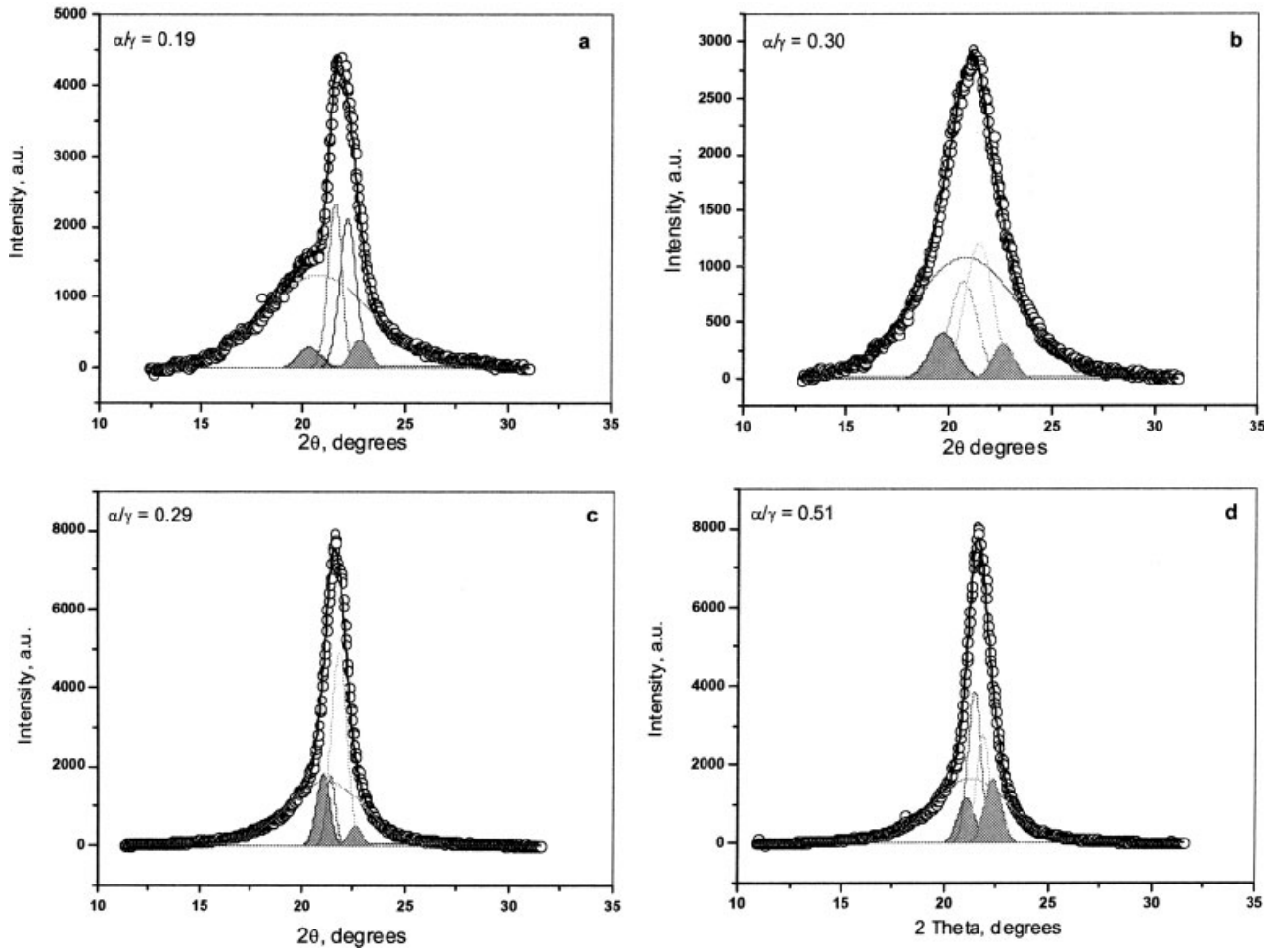

Figure 4 1D WAXS patterns of PA12 samples annealed for 1 h at 160°C and their fitting with Gaussian peaks: PA12 film (a) before and (b) after tensile testing and PA12 OC (c) before and (d) after tensile testing. The peaks of α-PA12 are shaded. The amorphous halo was modeled by one Gaussian.

proves the strong orientation in the PA12 OCs, the draw direction being vertical. Drawing the PA12 films to sample failure during the tensile test transforms the isotropic pattern in Figure 5(a) into the well-oriented pattern in Figure 5(c), which indicates that the external force is transferred to the crystalli-

TABLE III
Temperature Dependence of CI_{total} or ECI, CI_α, CI_γ, and the α/γ Polymorph Ratio Before and After Tensile Testing Resulting in Sample Failure

Sample and annealing conditions	Before tensile testing				After tensile testing			
	CI_α (%)	CI_γ (%)	CI_{total} or ECI	α/γ content	CI_α (%)	CI_γ (%)	CI_{total} or ECI	α/γ content
PA12 isotropic films								
120°C/1 h	4.1	26.9	31.0	0.18	12.3	26.1	38.4	0.47
120°C/3 h	6.6	27.0	33.6	0.24	9.2	27.5	36.7	0.33
140°C/1 h	7.5	26.0	33.5	0.29	10.1	28.3	38.4	0.36
160°C/1 h	6.0	31.3	37.3	0.19	9.1	30.2	39.3	0.30
PA12 OCs								
Without annealing	8.4	33.4	41.8	0.25	—	—	—	—[a]
80°C/1 h	9.4	31.9	41.3	0.29	14.9	28.3	43.1	0.53
100°C/1 h	12.8	38.0	50.8	0.34	19.4	32.9	52.3	0.59
120°C/1 h	14.5	36.6	51.1	0.39	20.9	32.4	53.3	0.65
140°C/1 h	13.3	39.3	52.6	0.34	18.2	32.9	51.1	0.55
160°C/1 h	11.5	37.8	49.3	0.30	17.6	33.9	51.6	0.52

[a] No data were available.

TABLE IV
Unit Cell Vectors and Corresponding *d*-Spacings Obtained from the 1D and 2D WAXS Patterns of Isotropic and Oriented PA12 Samples as a Function of Their Initial Annealing Before and After Tensile Testing That Resulted in Sample Failure

Sample and annealing conditions	$d_{\alpha 200}$		$d_{\alpha 002}$		$d_{\gamma 200}$		$d_{\gamma 001}$		$d_{\gamma 020}$	
	Before	After	Before	After	Before	After	Before	After	Before	After
PA12 isotropic films										
120°C/1 h	4.28	4.36	3.82	3.90	4.02	4.14	3.96	4.02	14.00[a]	13.68
120°C/3 h	4.25	4.36	3.82	3.86	4.02	4.12	3.92	4.02	—	—
140°C/1 h	4.22	4.32	3.83	3.86	4.04	4.14	3.91	4.00	—	—
160°C/1 h	4.21	4.38	3.79	3.82	4.01	4.18	3.90	4.03	13.34	12.99
PA12 OCs										
Without annealing	4.26	—	3.83	—	4.09	—	3.98	—	13.98	13.02
80°C/1 h	4.22	4.20	3.84	3.88	4.07	4.07	3.96	3.99	—	—
100°C/1 h	4.28	4.26	3.89	3.91	4.09	4.08	4.00	3.99	—	—
120°C/1 h	4.15	4.13	3.89	3.90	4.04	4.04	3.98	3.96	—	—
140°C/1 h	4.14	4.13	3.89	3.92	4.09	4.09	3.97	4.01	—	—
160°C/1 h	4.11	4.11	3.82	3.87	4.03	4.03	3.96	3.96	13.50	13.12

[a] The **b** vector of the γ form for some samples was obtained from the meridional (020) reflection of the respective 2D WAXS patterns.

tes. The 2D WAXS patterns of PA12 OCs upon drawing do not change in their symmetry; only the scattering intensity decreases, most likely because of the smaller sample cross-section.

As shown in Table IV, increasing the annealing temperature of PA12 films in the 120–160°C region leads to a decrease in $d_{\alpha 200}$, $d\gamma_{001}$, and $d_{\gamma 020}$ values, whereas the rest of the *d*-spacings remain constant. Drawing the films to sample failure generally results in a well-expressed growth of all *d*-spacings obtained from the equatorial reflections, whereas the $d_{\gamma 020}$ values drop. With the oriented PA12 samples, a clear trend toward diminution of $d_{\alpha 200}$ and $d_{\gamma 020}$ as a function of the annealing temperature was registered, the rest of the *d*-spacings remaining constant. The application of an external force changes only the $d_{\gamma 020}$ values, which are best revealed in the OC without annealing.

2D SAXS measurements

The evolution of the 2D SAXS patterns in isotropic and oriented PA12 samples as a function of the annealing temperature before and after tensile testing is given in Figure 6. All initial PA12 films display isotropic patterns similar to that in Figure 6(a). After the tensile test, the films annealed for 1 h at 120 and 140°C produce clear four-point scattering diagrams with a fiber structure [Fig. 6(b)], whereas the PA12 films with 3 h at 120°C and with 1 h at 160°C show only a vertical central streak and no evidence of coherent scattering at larger scattering vector (*s*) values [Fig. 6(c)].

The OCs have a completely different nanostructure [Fig. 6(d–f)]. The as-drawn cable and that annealed at 80°C show only a central streak [Fig. 6(d)] both before and after the tensile test. Annealing

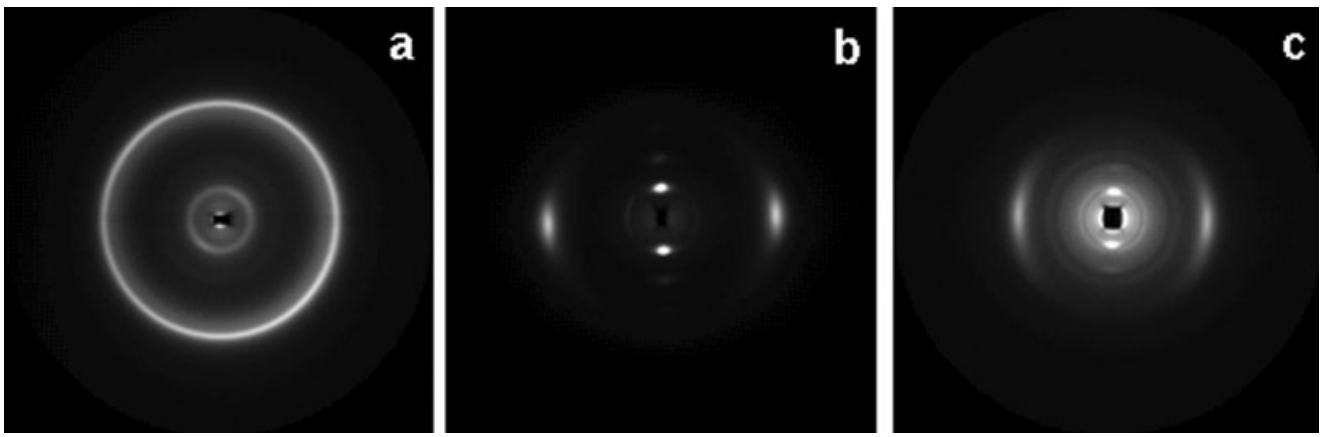

Figure 5 2D WAXS patterns of (a) a PA12 film annealed for 1 h at 160°C, (b) a PA12 OC without annealing, and (c) the previous PA12 film after the tensile test. All patterns were obtained at 30°C. The draw direction in panels b and c is vertical, and the *b* axis is the chain axis.

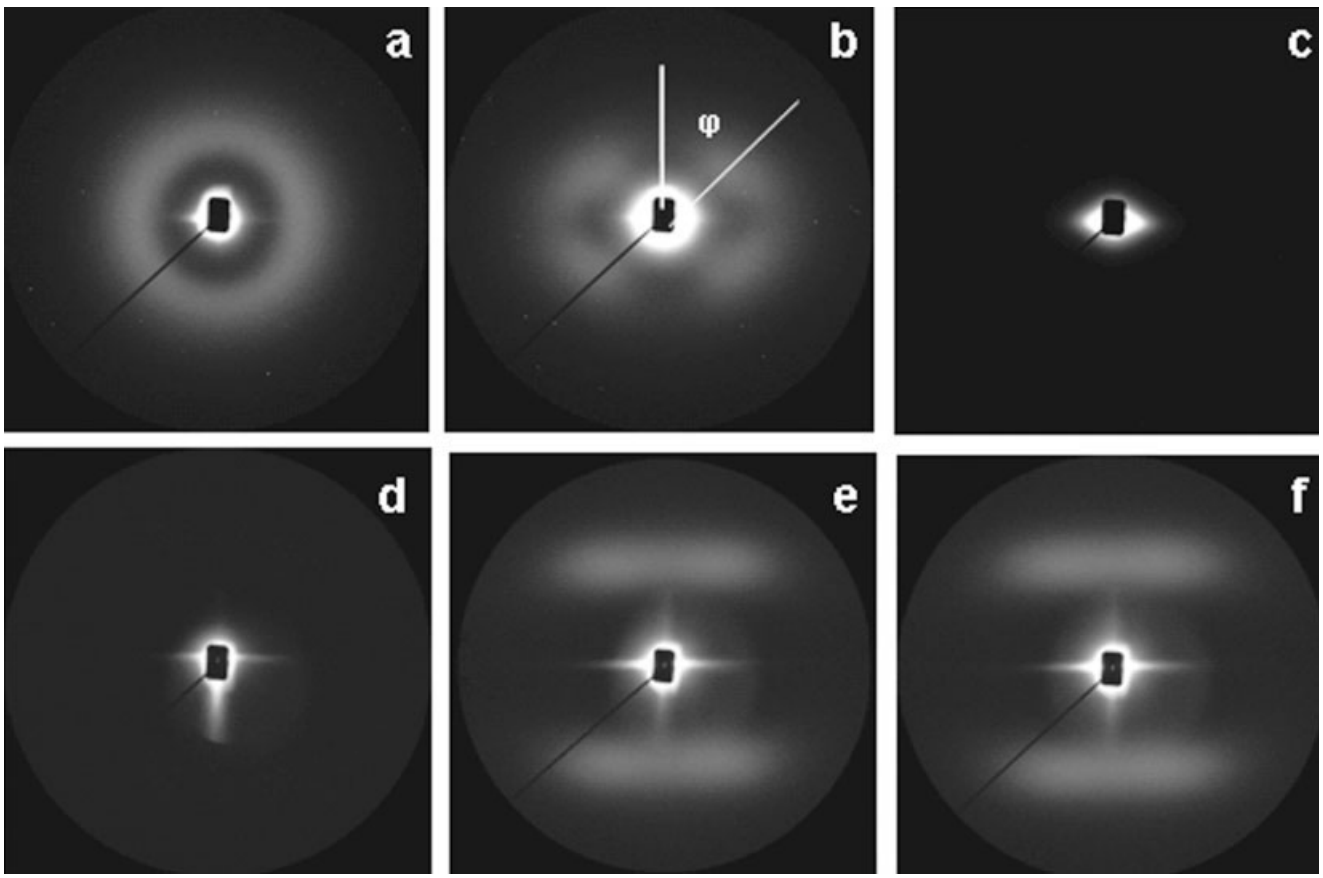

Figure 6 2D SAXS patterns of selected (a–c) isotropic films and (d–f) OCs with various annealing conditions before and after tensile testing: (a) an isotropic film annealed for 1 h at 140°C, (b) the same film after tensile testing, (c) a film annealed for 1 h at 160°C after tensile testing, (d) an OC without annealing, (e) an OC annealed for 1 h at 160°C, and (f) the same OC after tensile testing. All patterns were obtained at 30°C. The draw direction in the oriented patterns is vertical.

in the 100–160°C interval results in the appearance of coherent scattering typical of a microfibrillar structure [Fig. 6(e)], whose form does not change after the mechanical test [Fig. 6(f)].

More structural information can be extracted from the aforementioned 2D patterns after their processing: scanning the intensities in the radial direction provides quantitative information about the Bragg's long spacing (L_B) values and sample's scattering power, whereas the angular scan shows the intensity distribution in a given azimuthal angle range. Figures 7 and 8 display these data for PA12 films and OCs, respectively, as a function of the annealing temperature before and after tensile testing. Table V summarizes the L_B values of all samples studied.

Analyzing Figures 7 and 8 (the curves in parts a and b) shows that increasing the annealing temperature above 100°C results in a gradual increase of all L_B values (Table V) and of the scattering power, especially at 160°C. Stretching to mechanical failure in PA12 films leads, in general, to significantly lower scattering intensities and lower L_B values (1 h/120°C and 1 h/140°C) or to the complete disappearance of coherent scattering (3 h/120°C and 1 h/160°C). As shown in Figure 7(c), with these two samples, the applied external load resulted in a clear bimodal distribution of the scattered intensity with peaks at azimuthal angles of $\varphi = 45^\circ$ and $\varphi = 60^\circ$, respectively, φ being the angle between the draw direction and the normal to the lamellar surface (Fig. 6).

Similar trends were revealed with the OCs. [Fig. 8(a,b)], with the notable exception of the sample with 1 h at 140°C, which after the tensile test displayed higher scattering strength than that of the initial OC. The azimuthal scans of all OC patterns before and after the tensile test revealed curves very similar to those in Figure 8(c), indicating a four-point scattering diagram with $\varphi = 30^\circ$.

DISCUSSION

PA12 isotropic films

Analyzing the stress–strain curves in Figure 1(a) and the numerical data in Table I, we find that the annealed isotropic PA12 samples studied can be divided into two groups. Within each group, the mechanical properties can be considered very similar.

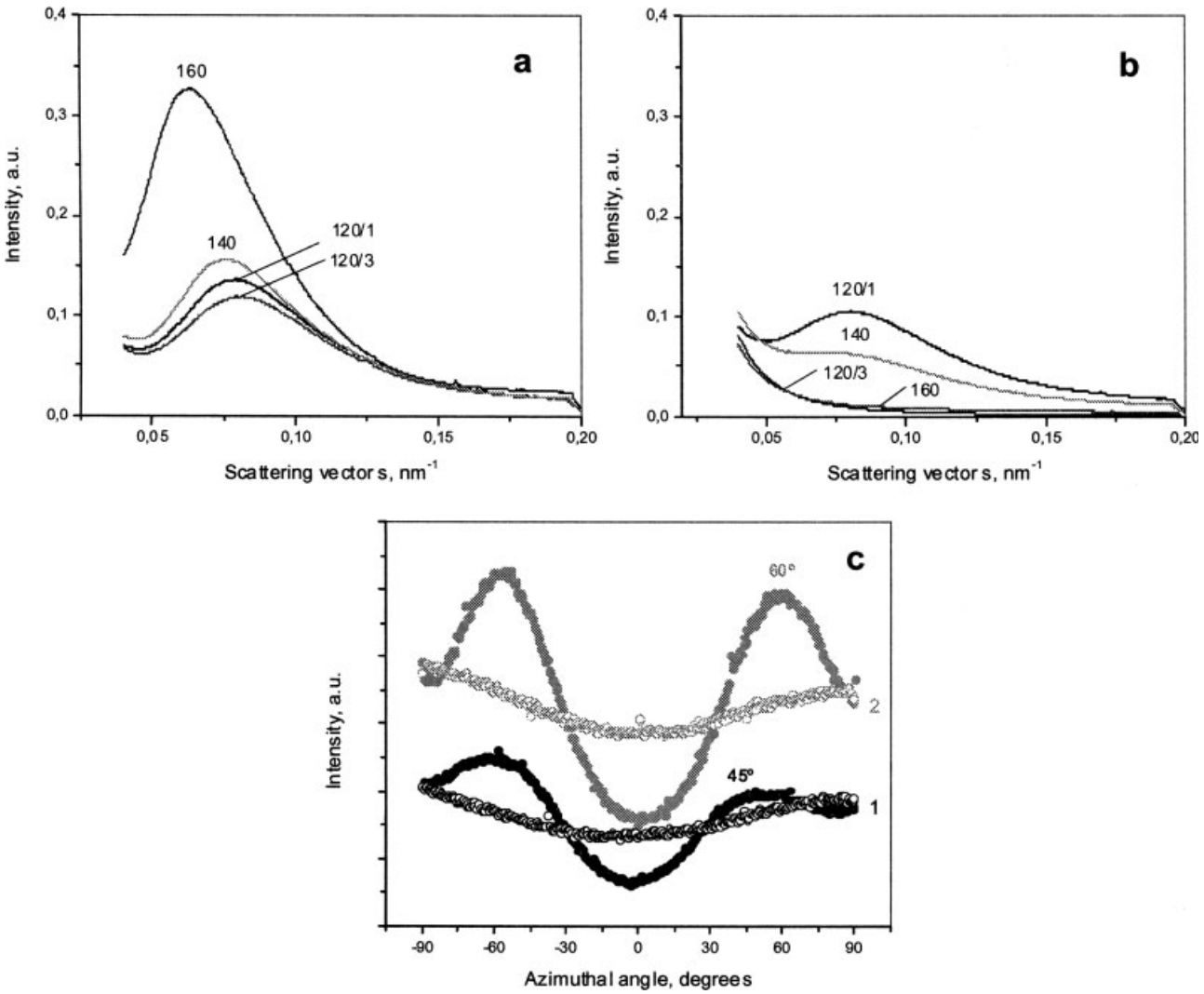

Figure 7 Slicing of 2D SAXS patterns of initially isotropic PA12 films: (a) raw 1D SAXS profiles as a function of the annealing temperature and duration before tensile testing, (b) the same profiles after tensile testing, and (c) azimuthal scans from −90 to +90° for samples with (1) annealing for 1 h at 120°C and (2) annealing for 1 h at 140°C. Open symbols represent data before tensile testing, and solid symbols represent data after tensile testing.

Thus, annealing for 1 h at 120 and 140°C results in ε_{br} values in the 190–200% range, σ_y being approximately 32 MPa and the E values being below 900 MPa. With the other two films annealed for 3 h at 120°C and for 1 h at 160°C, respectively, the ultimate strain drops to 50–60%. At the same time, E goes above 1.0 GPa, and σ_y also grows to approximately 35 MPa.

Relating the aforementioned mechanical behavior to the degree of crystallinity and the polymorph type (Table III) before tensile testing is not straightforward. On the one hand, increasing the annealing temperature from 120 to 160°C results in a 6% growth of CI_{total}, the largest difference being between 140 and 160°C. On the other hand, the α/γ content has its maximum at 140°C and goes back to the initial value of approximately 0.20 at 160°C. None of these changes can be linked directly to the mechanical performance of the respective samples. At the same time, however, Table IV shows that increasing the annealing temperature and its time duration leads to a slight but observable decrease of $d_{\alpha 200}$, $d_{\gamma 001}$, and $d_{\gamma 020}$ values. In the case of $d_{\alpha 200}$ and $d_{\gamma 001}$, this would mean a drop of the hydrogen-bond lengths within the α-PA12 and γ-PA12 sheets, respectively. In the case of $d_{\gamma 020}$, one deals with a well-expressed shrinkage of the γ-type unit cell along the chain axis. Both effects are related to a denser packing of the macromolecules in the crystalline domains, which is a probable explanation of the increase of σ_y as the annealing temperature grows.

All initially isotropic PA12 films after the tensile test showed 2D WAXS patterns with fiber symmetry similar to that in Figure 5(c), which indicated strong orientation of the crystallites along the draw direction. Most d-spacings increased after tensile testing (Table IV),

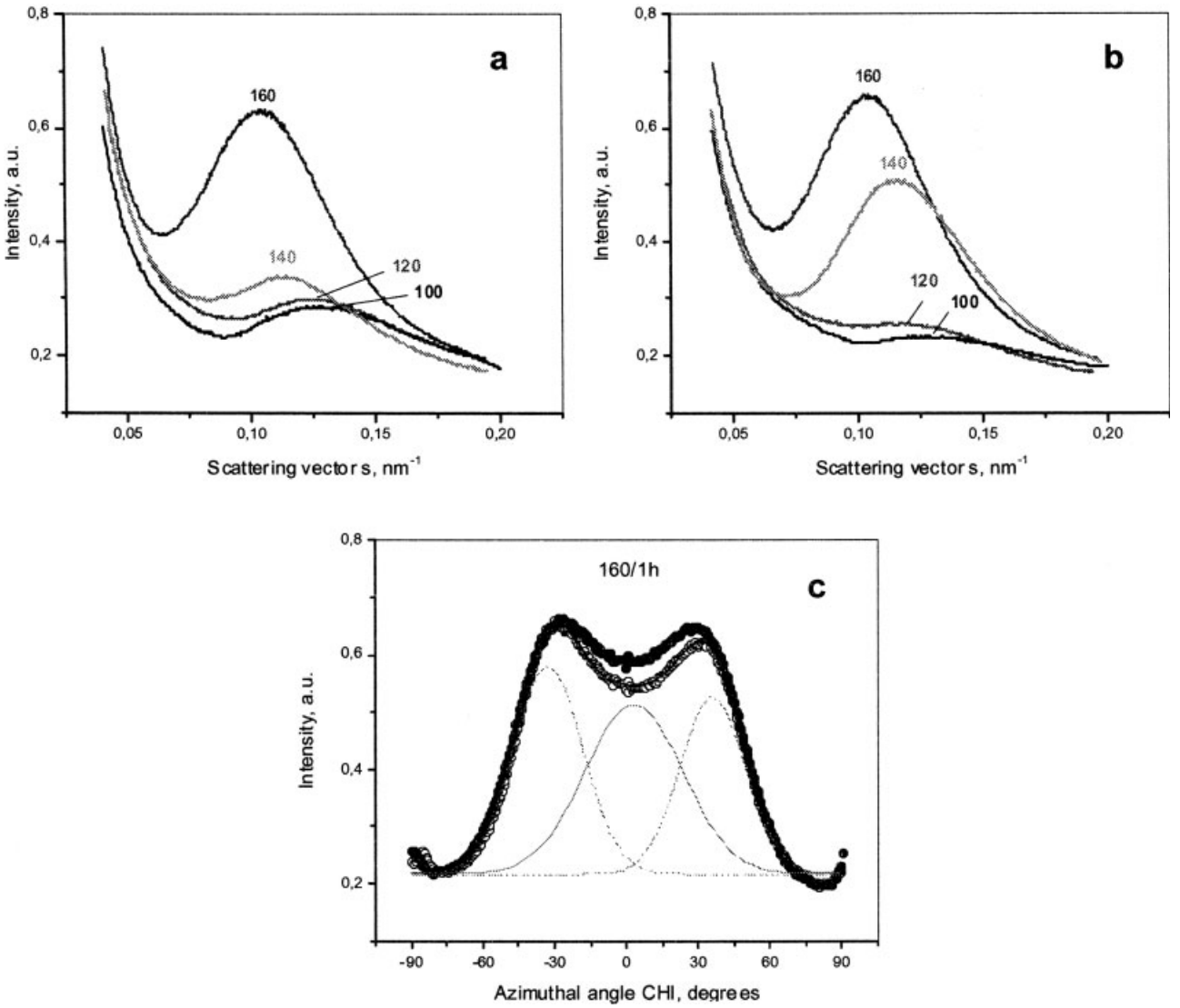

Figure 8 Slicing of 2D SAXS patterns of PA12 OCs: (a) raw 1D SAXS profiles as a function of the annealing temperature and duration before tensile testing, (b) the same profiles after tensile testing, and (c) azimuthal scans from -90 to $+90^\circ$ for a sample annealed for 1 h at 160°C. Open symbols represent data before tensile testing, and solid symbols represent data after tensile testing. The fit was made with the sample before tensile testing.

and this suggested a stress-induced unit cell expansion. Only $d_{\gamma 020}$ displayed some decrease. The same effect was observed in oriented PA6, too.[18] At this point, this experimental fact is not well understood.

The 2D and 1D SAXS data provide additional help in trying to understand the structure–property relationship in isotropic PA12 films before tensile testing. Figures 6(a) and 7(c) show that before the tensile test, the PA12 films can be considered isotropic with an almost uniform distribution of the scattered intensity along the circular 2D SAXS pattern. As a result of annealing, the scattering strength increases gradually between 120 and 140°C and with an abrupt jump between 140 and 160°C [Fig. 7(a)]. Exactly in the same way, the respective L_B values grow (Table V). Keeping in mind the CI_{total} values at the latter two temperatures (33.5 and 37.3%), we can hardly attribute the significant increase in L_B of 30 Å to lamellar thickening only, that is, to changes exclusively in the crystalline domains. Considering also the mechanical data, we think that a more logical explanation would be the supposition that annealing for 1 h at an annealing temperature greater than 140°C or for 3 h at 120°C results in the formation of certain amounts of a rigid amorphous phase that cannot be detected by WAXS, whose density, however, is very similar to that of the crystalline domains and is registered by SAXS.

We believe that the structural data after tensile testing support the supposition of the amorphous phase hardening above a certain annealing temperature. As already mentioned, the samples annealed

TABLE V
L_B Estimates for Differently Annealed Isotropic and Oriented PA12 Samples Before and After the Tensile Stress Test

Sample and annealing conditions	L_B estimate (Å)[a]	
	Before	After
Isotropic PA12 films		
120°C/1 h	126	122
120°C/3 h	128	—[b]
140°C/1 h	130	124
160°C/1 h	160	—
PA12 OCs		
Without annealing	—[b]	—[b]
80°C/1 h	—[b]	—[b]
100°C/1 h	77	78
120°C/1 h	78	78
140°C/1 h	84	85
160/°C 1 h	96	96

[a] The L_B values were determined from the raw SAXS profiles obtained after radial integration of the respective 2D images.
[b] No coherent SAXS scattering.

for 1 h at 120 and 140°C have similar ε_{br} values of approximately 190 and 200% versus the values of 50–60% for the samples with 3 h at 120 and 1 h at 160°C. This observation can be explained by the well-known concept that deformation of semicrystalline polymers takes place by unfolding of the flexible macromolecules found in the disordered domains between the stiff, ordered crystalline regions. Apparently, more flexible amorphous domains would correspond to higher ε_{br} values and vice versa.

A logical consequence of the aforementioned concept is that a part of the external force applied during the tensile test would be transferred to the crystalline domains, thus enabling stress-induced structural changes. A comparison of the α/γ content before and after tensile testing (Table III) suggests that the strongest γ-to-α-form transition as a result of drawing is registered after 1 h at 120°C and the lowest is registered after 1 h at 160°C. This leads to the unexpected conclusion that more flexible disordered domains would transfer to the adjacent crystalline domains a bigger part of the external force. The evolution of the stress at break (σ_{br}) as a function of the annealing temperature (Table I) helps explain this apparent paradox. Because of strain hardening, the films annealed for 1 h at 120 and 140°C have reached higher σ_{br} values, which have intensified the stress-induced γ-to-α polymorph transition.

More evidence of the appearance of a rigid amorphous phase as a result of annealing is found in the SAXS data in Figures 6 and 7. After the tensile test, the PA12 films annealed for 1 h at 120 and for 1 h at 140°C reveal four-point patterns similar to that in Figure 6(b). The structure that gives rise to such patterns is still being debated. According to some authors, the lamellar surface can tilt because of the progressive shear between the crystalline stems within the lamellae.[20–22] In this model, a two- or four-point pattern is obtained, depending on whether this surface is perpendicular to or tilted away from the chain axis (in this case coinciding with the draw direction), respectively. In a second group of models,[23,24] a four-point pattern is obtained when the lamellae are arranged in a lattice that resembles a checkerboard, and a two-point pattern is obtained when the lamellae are arranged in columns and the positions of the lamellae in the neighboring columns are not correlated. A recent extensive SAXS study on the deformation behavior of some thermoplastic polymers combines these two models. Thus, samples subjected to high deformations (250–500%) and thereafter unloaded consist of parallel crystalline lamellae tilted with respect to the draw direction. Under stress, however, there occurs a disruption of the tilted lamellae into smaller pieces. These fragments form a macrolattice with hexagonal order. When the elongation is increased beyond 250%, the lattice is transformed into an ensemble of microfibrils with little correlation in the lateral direction, and this gives rise to a two-point (lobe-type) pattern.[25] Another combined model explaining the four-point pattern in strained homopolymers was proposed very recently by Murthy and Grubb,[26] who introduced the concept of a three-dimensional lattice of tilted lamellae. A transition from a four-point SAXS diagram to a two-point SAXS diagram was also observed by Hernández et al.[27] by the stretching of a poly(ether ester) block copolymer with and without carbon nanotube reinforcement.

To explain the four-point patterns in the films annealed at 120°C for 1 h and at 140°C for 1 h after the tensile test, we supposed the presence of a flexible amorphous phase. The simplified scheme in Figure 9 visualizes the application of the tilted lamella deformation model with these samples. Underneath the respective lamellar structures, the scattering patterns produced by them are given.

Straining the isotropic PA12 films with a flexible amorphous phase during the mechanical test causes the arrangement of the random lamellae (1) into lamellar stacks oriented perpendicularly to the draw direction (2). The latter is present when the sample is still under stress in the testing machine. After sample failure, rupture of the tie molecules between the crystalline domains occurs. The release of the external force allows for the lamellar tilt to take place. From the azimuthal scans in Figure 7(c), it has been found out that the lamellar tilts are at approximately 45 (1 h/120°) and 60° (1 h/140°C). This is accompanied by a measurable decrease of L_B, which is expected in the case of relaxation. Figure 7(b)

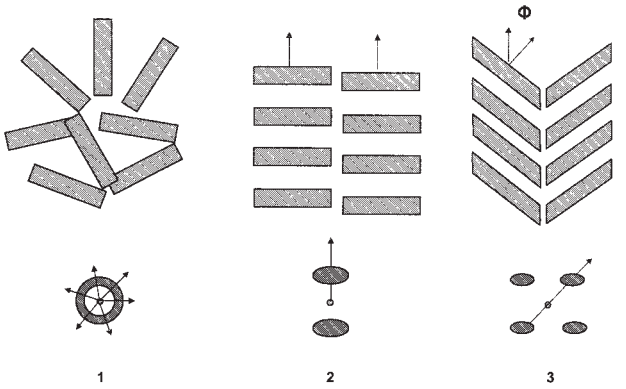

Figure 9 Simplified scheme of the stress-induced changes in isotropic PA12 films with a flexible amorphous phase: (1) random distribution of lamellae in the starting films resulting in spherical SAXS patterns, (2) oriented lamellar stacks before tensile testing resulting in two-point scattering patterns, and (3) tilting of the lamellar stacks after tensile testing producing four-point patterns. The shaded rectangles represent the crystalline domains of the lamellae.

shows also that stretching of the latter PA12 films results in a loss of scattering power.

After stretching of the harder PA12 films (3 h/120°C and 1 h/160°C), a complete loss of coherent SAXS scattering is observed [Figs. 6(c) and 7(b)]. The reason for this effect cannot be the disappearance of the denser domains because CI_{total} of the stretched samples increases compared to that in the respective samples before the tensile test. Most likely, as a result of stretching along the chain axis, the L_B values become too large to be registered by a sample-to-detector distance of 2.8 m. Evidently, no relaxation with an L_B decrease could occur after stress release. This fact supports the hypothesis that a harder amorphous phase is produced at a higher annealing temperature or with longer annealing times in PA12 films.

Oriented PA12 cables

The stress–strain curves of all PA12 cables [Fig. 1(b) and Table I] are characterized by a double yield. The two σ_y values change with the annealing temperature, reaching the highest values after annealing at 140°C, but it is difficult to trace any proportionality between these two parameters. All PA12 cables display similar ductility. As expected, the biggest ε_{br} was shown by the OC without annealing, and the smallest was shown by the OC annealed at 160°C. The E values were also affected by the annealing: in principle, the higher the annealing temperature was, the bigger the E values were.

Comparing the mechanical data of the OCs in Table I to the structural data extracted from the crystalline phase in Table III shows that the highest ultimate stress value of 266 MPa was obtained with the OC annealed at 140°C, which had the highest ECI of approximately 53%, containing at the same time the highest percentage of γ polymorph (close to 40%). Any decrease of ECI led to diminution of the ultimate stress values. The annealing temperature of 160°C seems to be higher than the optimum, causing some loss of crystallinity directly reflected in lower stress values (Tables I and III) Annealing the OCs in the range of 80–160°C leads to a general decrease of the $d_{\alpha 200}$ and $d_{\gamma 020}$ values, which indicates a denser packing of the macromolecules. As expected, all 2D WAXS patterns display a strong orientation along the draw direction (Fig. 5). This observation was confirmed by the 2D SAXS patterns in Figure 6. Some coherent scattering of lamellar structures was revealed only after annealing of the OCs at an annealing temperature greater than 100°C. As noted in the previous section, increasing the annealing temperature increases the scattering power of the OC before mechanical testing [Fig. 8(a)]. The jump in the scattered intensities between 1 h at 140 and 160°C was again attributed to the formation of a rigid amorphous phase not detectable by WAXS.

All curves obtained by azimuthal cuts of the 2D SAXS patterns of OCs annealed above 100°C are similar to that in Figure 8(c), which exemplifies the sample annealed at 160°C. These curves are different from those of the soft PA12 films after the tensile test [Fig. 7(c)]. The latter can be fitted with two Gaussians without any peak centered at 0°, thus indicating a pure four-point pattern attributable to the presence of tilted lamellae (Fig. 9). The curves of the OCs in Figure 8(c) need to be fitted with three Gaussians, the middle one being at 0° with respect to the chain axis direction. This finding supports the coexistence of two- and four-point patterns in the oriented PA12 samples. As mentioned previously, such patterns are typical of oriented semicrystalline fibers under stress whose scattering elements are arranged in a macrolattice. Figure 10 presents a schematic representation of the various structures and the respective SAXS patterns in PA12 OCs.

The initial OC without annealing, as obtained in the extruder line, is characterized by a nanostructure composed of laterally uncorrelated fibers with very large long spacings impossible to register with the maximum sample-to-detector distance in the beam line used. The scattering pattern is supposed to be of a two-point type, with its lobes being hidden behind the beam stop (structure 6 in Fig. 10). Annealing the OCs with free ends at a annealing temperature greater than or equal to 80°C results in relaxation whose macroscopic effect is the strong cable contraction observed with all OCs upon heating, with a drop in L_B being sufficient to reveal coherent SAXS scattering. Moreover, the significant increase in ECI registered in samples annealed at an annealing tem-

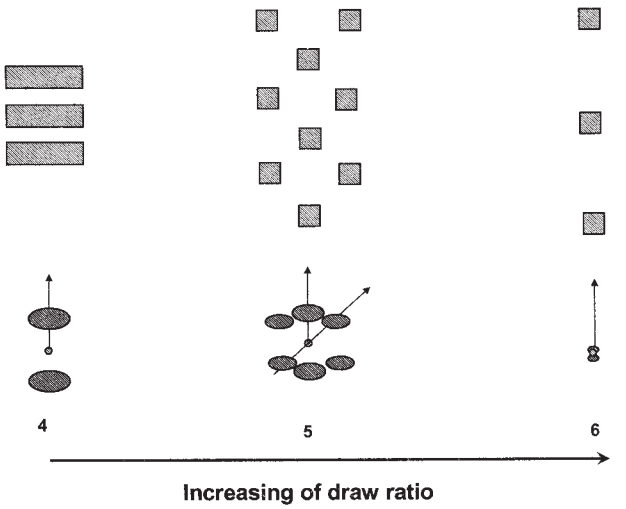

Figure 10 Simplified scheme of the stress-induced changes in PA12 OCs: (4) oriented lamellar stacks formed at a lower draw ratio resulting in two-point scattering patterns, (5) coexistence of two- and four-point patterns at a medium draw ratio arranging the scattering elements in the macrolattice, and (6) loss of lateral correlation and formation of fibrils with very large L_B. The shaded rectangles represent the crystalline domains of the lamellae.

perature greater than or equal to 100°C (Table III) may be related to the formation of some new crystalline domains of an α type appearing in the amorphous regions between the lamellae and leading to macrolattice formation similar to that shown in Figure 10 (structure 5). As a result, the L_B values drop significantly, and this makes possible their registration. The SAXS patterns display the coexistence of two- and four-point patterns. As shown in Table V, increasing the annealing temperature to 140°C and especially to 160°C starts a trend toward L_B growth. On the basis of the ECI data (Table III), this effect can be explained with lamellar thickening (up to 140°C) or with incipient fusion of some elements of the macrolattice (at 160°C), apparently from the α-PA12 polymorph.

With the PA12 OCs, we did not observe pure two-point patterns corresponding to structure 4 in Figure 10. The reason is that such a structure is expected at relatively low deformations. The preparation of OCs includes cold drawing to a high draw ratio, causing irreversible disruption of the crystalline lamellae to form a fibrillar structure. However, undisrupted oriented lamellar stacks giving two-point patterns have been undoubtedly registered at low deformation rates (ca. 50%) with a number of thermoplastic neat polymers and segmented copolymers.[25]

All OCs display ε_{br} values between 20 and 30%. Straining during the mechanical test leads to a well-pronounced γ-to-α-form transition (Table III). As shown in Figure 8(b), stretching results in a decrease of the scattering power with annealing temperatures of 100 and 120°C in comparison with the respective values before tensile testing [Fig. 8(a)]. With the samples annealed for 1 h at 140 and 160°C, there is an increase of the scattered intensity, which is much stronger in the former case. These results can be explained with the formation of additional amounts of a rigid amorphous phase. As shown in Table V, there are no changes in L_B after the mechanical test; that is, relaxation does not occur upon sample failure in any of the OCs. This finding could be related to an amorphous phase being hard enough to prevent any significant shrinkage of the microfibrils even at the lowest annealing temperature. This is in good agreement with the fact that the *d*-spacings of all OCs before and after tensile testing do not change significantly (Table IV). The only exception is the $d_{\gamma 020}$ value dropping strongly upon sample failure.

CONCLUSIONS

The PA12 isotropic films obtained by compression molding and the PA12 OCs obtained by consecutive extrusion and cold drawing contained predominantly the γ-crystalline form with some amounts of PA12 α modification, the fraction of the latter being larger in the oriented samples. The combination of solid-state ^{13}C-NMR with WAXS and SAXS from the synchrotron was very useful for obtaining reliable structural information about the polymorph transitions in PA12. Thus, the applied annealing caused an additional γ-to-α-form transition expressed in an increase of the α/γ content. Both isotropic and oriented PA12 samples showed a growth in the *E* and σ_y values as well as a decrease in ε_{br} values as the annealing temperatures increased. This behavior was explained, on a crystallographic level, by a denser packing of the macromolecules in the crystalline domains. All the obtained structural data allowed the supposition of the formation of a rigid amorphous phase in the annealed samples. The external stress applied during the tensile test led to additional stress-induced γ-to-α-form transitions in all PA12 samples accompanied by changes of the respective nanostructures.

References

1. Ulf, H.; Rohde-Liebenau, W. In Polymer Data Handbook; Mark, J. E., Ed.; Oxford University Press: New York, 1999; p 225.
2. Aharoni, S. M. n-Nylons: Their Synthesis, Structure and Properties; Wiley: New York, 1997; p 316.
3. Kohan, M. I. Nylon Plastics Handbook; Hanser: Munich, 1995.
4. Holmes, D. R.; Bunn, C. W.; Smith, D. J. J Polym Sci 1955, 17, 159.
5. Arimoto, H.; Ishibashi, M.; Hirai, M.; Chatani, Y. J Polym Sci Part A: Polym Chem 1965, 3, 317.
6. Fornes, T. D.; Paul, D. R. Polymer 2003, 44, 3945.

7. Samon, J. M.; Schultz, J. M.; Hsiao, B. S. Polymer 2000, 41, 2169.
8. Aleman, C.; Casanovas, C. Colloid Polym Sci 2004, 282, 535.
9. Li, L.; Koch, M.; de Jeu, W. H. Macromolecules 2003, 36, 1626.
10. Hiramatsu, N.; Hashida, S.; Hirakawa, S. Jpn J Appl Phys 1982, 21, 651.
11. Ishikawa, T.; Nagai, S.; Kasai, N. J Polym Sci Polym Phys Ed 1980, 18, 291.
12. Ishikawa, T.; Nagai, S.; Kasai, N. Makromol Chem 1981, 182, 977.
13. Hiramatsu, N.; Haraguchi, K.; Hirakawa, S. J Appl Phys 1983, 22, 335.
14. Northolt, M. G.; Tabor, B. J.; van Aartsen, J. J. J Polym Sci Part A-2: Polym Phys 1972, 10, 191.
15. Dencheva, N.; Nunes, T.; Oliveira, M. J.; Denchev, Z. J Polym Sci Part B: Polym Phys 2005, 43, 3720.
16. Denchev, Z.; Oliveira, M. J.; Carneiro, O. S. J Macromol Sci Phys 2004, 43, 143.
17. Dencheva, N.; Denchev, Z.; Oliveira, M. J.; Funari, S. S. J Appl Polym Sci 2007, 103, 2242.
18. Dencheva, N.; Nunes, T.; Oliveira, M. J.; Denchev, Z. Polymer 2005, 46, 887.
19. Mathias, L. J.; Johnson, C. G. Macromolecules 1991, 24, 6114.
20. Pope, D. P.; Keller, A. J Polym Sci Polym Phys Ed 1975, 13, 533.
21. Matyi, R. J.; Crist, B., Jr. J Polym Sci Polym Phys Ed 1978, 16, 1329.
22. Murthy, N. S.; Grubb, D. T. J Polym Sci Part B: Polym Phys 2003, 41, 1538.
23. Statton, W. O. J Polym Sci 1959, 16, 143.
24. Wilke, W.; Bratrich, M. J Appl Cryst 1991, 24, 645.
25. Stribeck, N.; Fakirov, S.; Apostolov, A. A.; Denchev, Z.; Gehrke, R. Macromol Chem Phys 2003, 204, 1000.
26. Murthy, N. S.; Grubb, D. T. J Polym Sci Part B: Polym Phys 2006, 44, 1277.
27. Hernández, J. J.; García-Gutiérrez, M. C.; Nogales, A.; Rueda, D. R.; Sanz, A.; Sics, I.; Hsiao, B. S.; Roslaniec, Z.; Broza, G.; Ezquerra, T. A. Polymer 2007, 48, 3286.